Supplemental Material

accompanying the manuscript

Inferring network connectivity from event timing patterns

Jose Casadiego,[1,2,*] Dimitra Maoutsa,[2,3,*] and Marc Timme[1,2,4,5]

[1] *Chair for Network Dynamics, Institute of Theoretical Physics and Center for Advancing Electronics Dresden (cfaed), Technical University of Dresden, 01062 Dresden, Germany*

[2] *Network Dynamics, Max Planck Institute for Dynamics and Self-Organization (MPIDS), 37077 Göttingen, Germany*

[3] *Artificial Intelligence Group, Department of Software Engineering and Theoretical Computer Science, Technical University of Berlin, 10587 Berlin, Germany*

[4] *Bernstein Center for Computational Neuroscience (BCCN), 37077 Göttingen, Germany*

[5] *Advanced Study Group, Max Planck Institute for the Physics of Complex Systems, 01069 Dresden, Germany*

CONTENTS

I. Simulating networks of spiking neurons 1

II. Performance for denser networks 3

III. Reconstruction in the presence of hidden units 3

IV. Reconstruction with external Poisson inputs 3

V. Generalization to reconstruction given bursting dynamics 3

VI. Robustness against misestimation of delays 4

VII. Further model-independent reconstruction methods 4
A. Cross-Correlations 4
B. Mutual Information 4
C. Spike-Triggered Average 5

VIII. Characterization of irregularity of spiking patterns 5

IX. Analysis of computational complexity 5

X. Implementations 5

References 6

I. SIMULATING NETWORKS OF SPIKING NEURONS

Most simulations were performed with Neural Simulation Tool NEST [1] with a temporal resolution $\delta t = 0.1\,\text{ms}$, refractory period $\tau^{\mathsf{ref}} = 2.0\,\text{ms}$ and transmission delay $\tau_{ij} = 1.5\,\text{ms}$, unless otherwise stated.

For networks of *Leaky Integrate-and-Fire (LIF)* neurons with current-based δ- and α-synapses, we employed the `'iaf_psc_delta'`, and `'iaf_psc_alpha'` models, in NEST terminology. These simulate typical LIF neurons, where the temporal evolution of the membrane potential of a neuron i is described by

$$C_i \frac{dV_i(t)}{dt} = -\frac{V_i(t)}{R_i} + I_i^{\mathsf{ext}} + I_i^{\mathsf{syn}}(t) \tag{1}$$

as long as the membrane potential is below the firing threshold V_{th}, $V_i < V_{\mathsf{th}}$. Coefficients C_i and R_i stand for the membrane capacitance and resistance of neuron i, I_i^{ext} for external tonic input currents, and $I_i^{\mathsf{syn}}(t)$ denotes synaptic input currents from the remaining simulated network

$$I_i^{\mathsf{syn}}(t) = \sum_{j \in \mathsf{Pre(i)}} \sum_p J_{ij} f\left(t - t_j^p - \tau_{ij}\right), \tag{2}$$

where $\mathsf{Pre(i)}$ stands for the set of presynaptic neurons of i, and t_j^p the p-th spike time of neuron j. Moreover, J_{ij} and τ_{ij} indicate the synaptic strength and transmission delay of the synapse from j to i, while function f describes the time course of the post-synaptic current induced by each received spike. For δ-synapses, each incoming spike evokes an instantaneous jump on the membrane potential of i, thus, the function f is a Dirac delta function,

$$f(t) = \delta(t), \tag{3}$$

while in α-coupling case [2] the post-synaptic current follows an exponential with rise time τ_{syn},

$$f(t) = \frac{1}{\tau_{\mathsf{syn}}} t \exp\left(1 - \frac{t}{\tau_{\mathsf{syn}}}\right). \tag{4}$$

In both cases, once the threshold V_{th} is reached or exceeded, neuron i is considered to emit a spike and the reset condition $V_i = V_i^{\mathsf{reset}}$ is applied, while its membrane potential remains clipped to that value for the time designated by the absolute refractory period, τ^{ref}.

For simulations of *Hodgkin-Huxley (HH)* neuronal networks, we used the `'hh_cond_exp_traub'` model [3] according to NEST nomenclature. Here, the net current flowing into the membrane of neuron i, consists of ionic currents flowing through the voltage-gated sodium, and potassium channels, denoted by I_{Na} and I_{K}, current flowing through the voltage-independent leakage channel, I_{L},

* J.C. and D.M. contributed equally to this work.

added to synaptic, I_i^{syn}, and externally applied tonic currents, I_{ext}. Both sodium and potassium channels follow HH dynamics [4], with g_{Na} and g_{K} denoting the respective conductances, E_{Na} and E_{K} the respective equilibrium (reversal) potentials, while m and h indicate the sodium channel activation and inactivation state variables, and n the potassium channel activation state variable, i.e. the probability that these channels are open/closed. For the leakage current, I_{L}, the relevant conductance is g_{L} and the equilibrium potential E_{L}.

$$
\begin{aligned}
C_i \tfrac{dV_i(t)}{dt} &= -I_{\mathsf{Na}} - I_{\mathsf{K}} - I_{\mathsf{L}} - I_i^{\mathsf{syn}} + I_{\mathsf{ext}} \\
I_{\mathsf{Na}} &= g_{\mathsf{Na}} m^3 h \left(V_i - E_{\mathsf{Na}}\right) \\
I_{\mathsf{K}} &= g_{\mathsf{K}} n^4 \left(V_i - E_{\mathsf{K}}\right) \\
I_{\mathsf{L}} &= g_{\mathsf{L}} \left(V_i - E_{\mathsf{L}}\right) \\
I_i^{\mathsf{syn}} &= g_i^{\mathsf{syn,ex}}(t) \left(V_i - E_{\mathsf{syn}}^{\mathsf{ex}}\right) + g_i^{\mathsf{syn,inh}}(t) \left(V_i - E_{\mathsf{syn}}^{\mathsf{inh}}\right) \\
g_i^{\mathsf{syn,ex}}(t) &= \sum_{\substack{j \in \mathsf{Pre(i)} \\ j \in \mathcal{E}}} \sum_p J_{ij} \exp\left(-\frac{t - t_j^p - \tau_{ij}}{\tau_{\mathsf{syn}}^{\mathsf{ex}}}\right) \\
g_i^{\mathsf{syn,inh}}(t) &= \sum_{\substack{j \in \mathsf{Pre(i)} \\ j \in \mathcal{I}}} \sum_p J_{ij} \exp\left(-\frac{t - t_j^p - \tau_{ij}}{\tau_{\mathsf{syn}}^{\mathsf{inh}}}\right)
\end{aligned}
\tag{5}
$$

The synaptic input current in (5) is given by the algebraic sum of excitatory and inhibitory synaptic currents. Each is a product of the synaptic conductance time course, $g_i^{\mathsf{syn,ex}}(t)$ or $g_i^{\mathsf{syn,inh}}(t)$, and the reversal potential driving force, namely the difference between the membrane and the relevant synaptic reversal potential, $E_{\mathsf{syn}}^{\mathsf{ex}}$ or $E_{\mathsf{syn}}^{\mathsf{inh}}$. In turn, each synaptic conductance is described by a sum of exponentials with peak amplitude J_{ij}, and time constant $\tau_{\mathsf{syn}}^{\mathsf{ex}}$ or $\tau_{\mathsf{syn}}^{\mathsf{inh}}$, each starting at time t_j^p a presynaptic neuron j emits its p-th spike, plus the transmission delay to i, τ_{ij}. The sum runs over the set of excitatory neurons, $\mathcal{E}$, for $g_i^{\mathsf{syn,ex}}(t)$, and similarly over the set of inhibitory neurons, $\mathcal{I}$, for $g_i^{\mathsf{syn,inh}}(t)$, that are additionally presynaptic to i, $j \in \mathsf{Pre(i)}$.

Furthermore, the dimensionless activation/inactivation state variables depend non-linearly on the membrane potential through the voltage-dependent transition rates, $\alpha_X$and β_X, with $X \in \{m, h, n\}$:

$$
\begin{array}{l}
\frac{dm}{dt} = \alpha_m\left(V_i\right)(1-m) - \beta_m\left(V_i\right) m \\
\frac{dh}{dt} = \alpha_h\left(V_i\right)(1-h) - \beta_h\left(V_i\right) h \\
\frac{dn}{dt} = \alpha_n\left(V_i\right)(1-n) - \beta_n\left(V_i\right) n
\end{array}
\quad , \tag{6}
$$

where, in turn, the transition rates are given by

$$
\begin{aligned}
\alpha_m\left(V_i\right) &= \tfrac{0.032(13-V_i)}{e^{(13-V_i)/4}-1} \\
\beta_m\left(V_i\right) &= 0.28 \tfrac{V_i-40}{e^{(V_i-40)/5}-1} \\
\alpha_h\left(V_i\right) &= 0.128\, e^{(17-V_i)/18} \\
\beta_h\left(V_i\right) &= \tfrac{4}{1+e^{(40-V_i)/5}} \\
\alpha_n\left(V_i\right) &= \tfrac{0.032(15-V_i)}{e^{(15-V_i)/5}-1} \\
\beta_n\left(V_i\right) &= 0.5\, e^{(10-V_i)/40}.
\end{aligned}
\tag{7}
$$

For networks of adaptive *Exponential Integrate and Fire neurons (aEIF)* (cf. Suppl.V) we used the BRIAN2 simulator [5]. Formally the dynamics of the neuronal model are captured by two coupled ordinary differential equations, describing the evolution of the membrane potential V and an adaptation current w, which accounts for spike-triggered and sub-threshold adaptation

$$
\begin{aligned}
C \tfrac{dV}{dt} &= -g_L\left(V - E_L\right) + g_L \Delta_T \exp\left(\tfrac{V - V_T}{\Delta_T}\right) + I - w \\
\tau_w \tfrac{dw}{dt} &= a\left(V - E_L\right) - w,
\end{aligned}
\tag{8}
$$

where C the membrane capacitance, I synaptic or external current, g_L leak conductance, E_L resting potential. V_T denotes the firing threshold, while Δ_T is a slope factor that determines the sharpness of the threshold. The adaptation current w evolves in a slower time-scale than V, τ_w, with a characterizing the level of subthreshold adaptation.

Every time the membrane voltage V reaches the threshold V_T, a spike is emitted and the voltage resets to E_L, while the adaptation current increases by an amount b.

The model is capable of generating bursting behavior. In particular, in our simulations, following [6] we employ the following parameters to induce periodic bursting activity: $C = 100$ pF, $g_L = 10$ nS, $E_L = -70.6$ mV, $V_T = -50.4$ mV, $V_{\mathsf{th}} = -40.4$ mV $\tau_w = 100$ ms, $\Delta_T = 2$ mV, $a = 0.001$ nS, $b = 0.15$ nA, $V_r = -45$ mV, $I = \mathcal{U}(0.99, 1.01)$ nA, $N_{\mathsf{exc}} = 25$, $N_{\mathsf{inh}} = 25$, $p = 0.1$, Sim.Time= 150 s.

General parameters for data sets used in the main manuscript are shown in S1.

Fig.	N_{exc}	N_{inh}	J_{exc}	J_{inh}	p	Sim. Time	Input
2b	50	50	0.3 mV	-0.3 mV	0.1	50 s	$\mathcal{U}(1.2, 1.4)$pA
3	n/a	100	n/a	(-0.3,-5.0,-9.0) mV	0.1	500 s	$\mathcal{U}(1.4, 1.6)$pA
4a	50	50	0.5 mV	-2.0 mV	0.1	250 s	$\mathcal{U}(240.0, 280.0)$pA
4b	50	50	30.0 nS	-300 nS	0.1	250 s	$\mathcal{U}(150.0, 152.0)$pA
4c-d	50	50	0.5 mV	-0.5 mV	0.1	200 s	$\mathcal{U}(1.2, 1.4)$pA
5	1500	500	0.005 mV	-0.025 mV	0.1	800 s	$\mathcal{U}(1.03, 1.06)$pA

Table S1. **Simulation parameters for figures in main manuscript.** N_{exc}: number of excitatory neurons, N_{inh}: number of inhibitory neurons, J_{exc}: coupling strength of excitatory neurons, J_{inh}: coupling strength of inhibitory neurons and p: connection probability. Here $\mathcal{U}(\cdot)$ stands for uniform distribution.

Further neuronal parameters considered in the simulations:

- **Leaky integrate and fire neurons with delta/alpha synapses:** membrane capacitance $C = 250\,pF$, membrane time constant $\tau_{\mathsf{m}} = 20\,ms$, synaptic time constant $\tau_{\mathsf{syn}} = 0.5\,ms$ (where relevant), refractory period $\tau^{\mathsf{ref}} = 2.0\,ms$, firing threshold $V_{\mathsf{th}} = 20\,mV$, and reset potential $V^{\mathsf{reset}} = 0\,mV$.
- **Hodgkin-Huxley neurons:** membrane capacitance $C = 600\,pF$, synaptic time constants for excitatory $\tau^{\mathsf{ex}}_{\mathsf{syn}} = 0.5\,ms$, and inhibitory synapses $\tau^{\mathsf{inh}}_{\mathsf{syn}} = 0.5\,ms$, reversal potentials $E_{\mathsf{L}} = -56.0\,ms$, $E_{\mathsf{Na}} = 55.0\,ms$, $E_{\mathsf{K}} = -90.0\,ms$, and conductances $g_{\mathsf{L}} = 200.0\,nS$, $g_{\mathsf{Na}} = 7000.0\,nS$, and $g_{\mathsf{K}} = 1800.0\,nS$, and constant external input current $I_{\mathsf{e}} = 80.0\,pA$.

II. PERFORMANCE FOR DENSER NETWORKS

Reconstructing networks of fixed size and regular dynamics ($CV = 0.1$) with different connection probabilities p revealed that denser connectivities have minute effect on the necessary number of events for achieving successful reconstructions, cf. S1, while reconstructions employing Generalized Linear Models (GLM)[7] are imperfect for dense networks, independently of the observation time T, Figure S1b.

III. RECONSTRUCTION IN THE PRESENCE OF HIDDEN UNITS

Hidden (or unobservable) units generally affect the dynamics of measured units in nonquantifiable ways, unless more information about the hidden units is provided. Thus, such units may correlate or decorrelate the dynamics of measured units and lead to the recovery spurious interactions among them. Our numerics nevertheless show that, for increasing fractions of observed units, the recovery of spurious links is suppressed by taking into account larger numbers of recorded events. Specifically, our results suggest that observed fractions as small as 25% of the units may already reveal more accurate network structures than random guessing, Figure S2.

IV. RECONSTRUCTION WITH EXTERNAL POISSON INPUTS

To understand how our theory behaves on noisy dynamics, we coupled additional external inputs emulating neurons producing spikes with Poisson statistics on each neuron in the recurrent network. Specifically, each neuron in the recurrent network receives a unique stream of spikes following Poisson statistics.

In particular, we studied how the rate ν and the strength J_{noise} of the Poisson inputs affect the reconstruction results. The rate ν controls the average number of spikes produced per unit of time and the strength J_{noise}determines the effect of each spike when it arrives on a neuron of the recurrent network. However, here instead of focusing on ν, we focused on the variable λ which represents a percentage of the necessary frequency ν_{th} to raise the resting state potential of neurons to their threshold value. So, for instance, $\lambda = 0.1$ indicates that the rate employed in simulations is a 10% of the necessary rate to maintain the membrane potential at the threshold value.

We observed that even for moderate noise, $\lambda = 0.2$, accurate reconstruction is feasible if J_{noise} is relatively small compared to strength of synaptic inputs within the recurrent network ($\approx 33\%$). Yet, increasing J_{noise} decreases the ability of our theory to accurately reveal the incoming connections, Figure S3.

V. GENERALIZATION TO RECONSTRUCTION GIVEN BURSTING DYNAMICS

Here, we extend our inference framework to settings where the spiking units exhibit bursting dynamics, i.e. intermittent high-frequency firing followed by a quiescence period. Physiologically, neuronal bursting is attributed to interaction of a fast spike generating process and a slower ionic mechanism that modulates burst occurrence and duration [8]. In terms of dynamics, neuronal models exhibiting bursting are described by fast-slow systems, where fast state variables account for the spiking activity, while slow variables regulate the onset of bursting [9]. Our inference method, in a regular spiking setting, relies on the approximation of the function that regulates the length of an inter-spike interval. Thus, for settings with bursting firing, the length of a bursting pe-

riod, ΔB, i.e. the time interval between two consecutive burst onsets (Figure S4a), effectively replaces the notion of an inter-spike interval, ΔT.

Let us denote with $B_{i,m}$ the ordered set of b spike times of neuron i that occurred during its m-th bursting period, i.e.

$$B_{i,m} = \{t_{i,m,1},\, t_{i,m,2},\, \ldots,\, t_{i,m,b}\}.$$

We express the duration of the m-th bursting period as the difference between the first spike times of the sets $B_{i,m}$ and $B_{i,m-1}$,

$$\Delta B_{i,m} = t_{i,m,1} - t_{i,m-1,1}\,.$$

The notion of cross-spike intervals remains the same as previously, keeping in mind that, here, we are interested in the cross-spike intervals between the onset of the m-th burst and a spike emitted by j,

$$w^i_{j,k,m} = t_{j,p,\cdot} - t_{i,m-1,1}\,.$$

In the same spirit, events here are defined as

$$e_{i,m} := \left[vec\left(W^i_m\right),\, \Delta B_{i,m}\right]^{\mathrm{T}} \in \mathbb{R}^{\left(NK^i+1\right)}, \qquad (9)$$

where W^i_m and K^i follow the same definitions as in the main letter.

By replacing these aforementioned terms, the framework for reconstructing incoming connections remains the same as in the main article.

To demonstrate the modified approach, we simulate networks of adaptive exponential integrate-and-fire (aEIF) neurons [10] in a parameter regime where each neuron individually emits bursts periodically. By considering events described by Eq. 9 reconstructions effectively reveal the underlying synaptic interactions in the limit of numerous employed events (Fig. S4b).

VI. ROBUSTNESS AGAINST MISESTIMATION OF DELAYS

Synaptic transmission delays $\tau_{ij} \in \mathbb{R}^+$ from pre to postsynaptic neurons may play an important role in revealing synapses. Although transmission delays do not appear in (9) (cf. main manuscript), they essentially determine the exact location of events in the event space (since inaccurate delays may elicit mismatches of ISI-CSI pairs). Yet, reconstruction is still successful, even if the τ_{ij} are estimated inaccurately, again with improving quality for increasing number of spikes taken into account, Figure S5c. Defining the error function

$$E_2(\tau_{ij}) = \frac{\sum_{m=1}^{M}\left(\Delta T_{i,m} - \widehat{\Delta T}_{i,m}(\tau_{ij})\right)^2}{\max_{\tau_{ij}}\left(\sum_{m=1}^{M}\left(\Delta T_{i,m} - \widehat{\Delta T}_{i,m}(\tau_{ij})\right)^2\right)}, \qquad (10)$$

where $\widehat{\Delta T}_{i,m}(\tau_{ij})$ is the approximation of $\Delta T_{i,m}$ by our approach for a specific τ_{ij}, we may study the effect of selecting different delays for the same spike train. Specifically, different τ_{ij} produce different sets of events , and thereby different estimations of $\widehat{\Delta T_{i,m}}(\tau_{ij})$. In particular, varying τ_{ij} shows the error function (10) exhibits a global minimum approximately at the actual transmission delay employed in simulations, Figure S5d. Such result suggest that our approach may also be used to find estimates of average transmission delays.

VII. FURTHER MODEL-INDEPENDENT RECONSTRUCTION METHODS

We compared the proposed framework with existent model-independent approaches frequently employed to identify network interactions.

A. Cross-Correlations

We calculated the cross-correlation between spiking activity of neurons i and j, by convolving their time-resolved spike trains. In particular, we employed a $b = 5\,ms$ binning window to convert the spiking data to spike count signals $s_i\,[t]$ and $s_j\,[t]$. Subsequently, the cross-correlation was computed as the maximum of the convolved signals $s_i\,[t]$ and the time reversed version of $s_j\,[t]$

$$CC_{i,j} = \max\left(s_i\,[t] * s_j\left[\frac{T}{b} - t\right]\right),$$

where T stands for the total duration of the spike train.

For computational efficiency, the convolution was computed in the Fourier domain, as a product of the Fourier transformed signals.

B. Mutual Information

We evaluated the (delayed) mutual information between the spike train of neurons i and j with the information theoretic toolbox Pyentropy [**?**]. Given the spike trains of both neurons, we computed their time-resolved signals, $s_i\,[t]$ and $s_j\,[t]$, by employing a binning window of $b = 5\,ms$, delaying thereby the observed spike times of i by the transmission delay from i to j, τ_{ij}. We evaluated the information entropy of the binned spike train of i, $H\,(s_i)$, by employing a naive estimation of the probability distributions

$$H\,(s_i) = -\sum_{c=0}^{C} p\,(c)\log_2 p\,(c)\,,$$

where c runs over C observed spike counts in the binned spike train $s_i[t]$, and the probabilities of c spike counts,

$p(c)$, were approximated by relative frequencies, $p(c) \approx f(c) \equiv \frac{n_c}{\frac{T}{b}}$, where n_c stands for the number of bins with c spikes, and T for the overall spike train duration.

Similarly, we computed the conditional entropy of the spike train of i given the spike train of j, $H(s_i \mid s_j)$, according to

$$H(s_i \mid s_j) = -\sum_{l=0}^{L} p(l) \sum_{c=0}^{C} p(c|l) \log_2 p(c|l),$$

where the outer summation runs over the L observed spike counts in the binned spike train s_j, where $p(l)$ the probability of observing l spike counts in the binned spike train s_j, and $p(c|l)$the probability of observing c spike counts in s_i,given l spikes in s_j. Again the probabilities where approximated by relative frequencies.

The (delayed) mutual information between the spike train of j and the (delayed) spike train of i was finally obtained as the reduction of the entropy of s_i by considering the conditional entropy $H(s_i \mid s_j)$,

$$I(s_i; s_j) = H(s_i) - H(s_i \mid s_j).$$

C. Spike-Triggered Average

We characterized the spike-triggered average for the binned spike trains of neurons i and j, $s_i[t]$ and $s_j[t]$, (with binning window $b = 0.1\,ms$) by averaging $s_j[t]$ over a window of size $w = 10\,ms$ preceding the spikes emitted by i. For the sake of brevity, we denote the signal s_j over the window w preceding each spiking event occurring at t_i^l of neuron i with the symbol $\mathbf{s_j^w}\left[\mathbf{t_i^l}\right]$.

Thus we calculated

$$\mathbf{STA_{ij}^w} = \frac{1}{M_i} \sum_{l=1}^{M_i} \mathbf{s_j^w}\left[\mathbf{t_i^l}\right] s_i\left[t_i^l\right],$$

where the summation runs over the M_i observed inter-spike intervals of neuron i, and $\mathbf{STA_{ij}^w} \in \mathbb{R}^{b \cdot w}$.

Finally, to determine a connectivity estimation from neuron j to i, we extract the maximum of the spike triggered average vector

$$STA_{ij} = \max\left(\mathbf{STA_{ij}^w}\right).$$

VIII. CHARACTERIZATION OF IRREGULARITY OF SPIKING PATTERNS

We characterized the temporal irregularity of firing of neuron i with the Coefficient of Variation (CV), defined as the ratio of the standard deviation of inter-spike intervals of i, σ_i, to their average duration μ_i

$$CV_i = \frac{\sigma_i}{\mu_i}.$$

The CV is a strictly positive quantity, with vanishing values indicating a completely regular firing pattern, and with values exceeding 0.5 designating irregular firing activity.

The spiking activity of the entire network was characterized by the mean of the individual CVs of the N observed neurons in the circuit

$$CV = \frac{1}{N} \sum_{i=1}^{N} CV_i.$$

IX. ANALYSIS OF COMPUTATIONAL COMPLEXITY

For the reconstruction of the incoming connectivity of any single unit, we perform the following computations with the mentioned computational complexity. In the following, M is the maximum number of recorded inter-event intervals per unit, N the number of recorded units, K maximum number of cross-event intervals per unit. Therefore every event is a vector of dimension $(NK+1)$ (cf. Equation 6 in main manuscript).

- Construction of M cross-event interval matrices $W_m^i \in \mathbb{R}^{NK}$, $m = 1,\ldots,M$ (cf. Equation 4 and 5 in main manuscript): $\mathcal{O}(MNK)$
- Computation of distances among M events (cf. Equation 7 in main manuscript): $\mathcal{O}\left((MNK)^2\right)$
- Selection of reference event with minimum distance to all the other events (cf. Equation 7 in main manuscript): $\mathcal{O}\left(M^2\right)$
- Construction of the linear system of equations (cf. Equation 9 in main manuscript): $\mathcal{O}(MNK)$
- Solution of the over-determined $(M > NK)$ linear system of equations with Singular Value Decomposition: $\mathcal{O}\left(M^2NK + (NK)^3\right)$[11]

Asymptotically, the terms $\mathcal{O}\left((MNK)^2 + (NK)^3\right)$ dominate, and since here we consider only over-determined systems of equations, where M>NK, the overall computational complexity is $\mathcal{O}\left((MNK)^2\right)$. Thus the computational bottleneck of our framework is the calculation of the distances among the events in the event space.

X. IMPLEMENTATIONS

Exemplary implementation of network simulation and reconstruction is available at: https://gitlab.com/di.ma/Connectivity_from_event_timing_patterns.

[1] M.-O. Gewaltig and M. Diesmann, Scholarpedia **2**, 1430 (2007).
[2] A. Morrison, S. Straube, H. E. Plesser, and M. Diesmann, Neural Comput. **19**, 47 (2007).
[3] R. D. Traub and R. Miles, *Neuronal networks of the hippocampus* (Cambridge University Press, 2008).
[4] A. L. Hodgkin and A. F. Huxley, J. Physiol. **117**, 500 (1952).
[5] M. Stimberg, D. F. M. Goodman, V. Benichoux, and R. Brette, Front. Neuroinform. **8**, 6 (2014).
[6] R. Naud, N. Marcille, C. Clopath, and W. Gerstner, Biol. Cybern. **99**, 335 (2008).
[7] Y. V. Zaytsev, A. Morrison, and M. Deger, J. Comput. Neurosci. **39**, 77 (2015).
[8] R. Krahe and F. Gabbiani, Nat. Rev. Neurosci. **5**, 13 (2004).
[9] E. M. Izhikevich, *Dyn. Syst.* (MIT Press, Cambridge, 2007) p. 441.
[10] R. Brette and W. Gerstner, J. Neurophysiol. **94**, 3637 (2005).
[11] G. H. Golub and C. F. Van Loan, *Matrix computations* (Johns Hopkins University Press, 1996) p. 694.

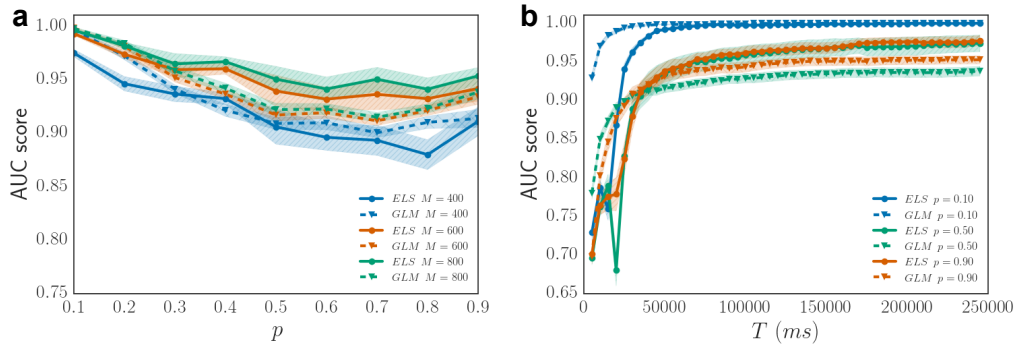

Figure S1. **Local samplings reveal synaptic connections of denser networks with minimal extra effort.** Quality of reconstruction measured in AUC score for ESL and GLM methods (**a**), versus connection probability p for M observed inter-spike intervals per neuron, and (**b**), versus simulation time T for networks of LIF-δ neurons of $N = 100$ with $N_{exc} = 50$ excitatory and, $N_{\text{inh}} = 50$ inhibitory connections for regular dynamics ($CV = 0.1$), $J_{\text{exc}} = \frac{0.5}{p \cdot 10}$ mV and $J_{\text{inh}} = -4 \cdot J_{\text{exc}}$, and transmission delays $\tau = 2.0\,ms$. The input currents were randomly selected from the uniform distribution $I_i \in [1.04, 1.06]$ pA for all $i \in \{1, 2, \ldots, N\}$.

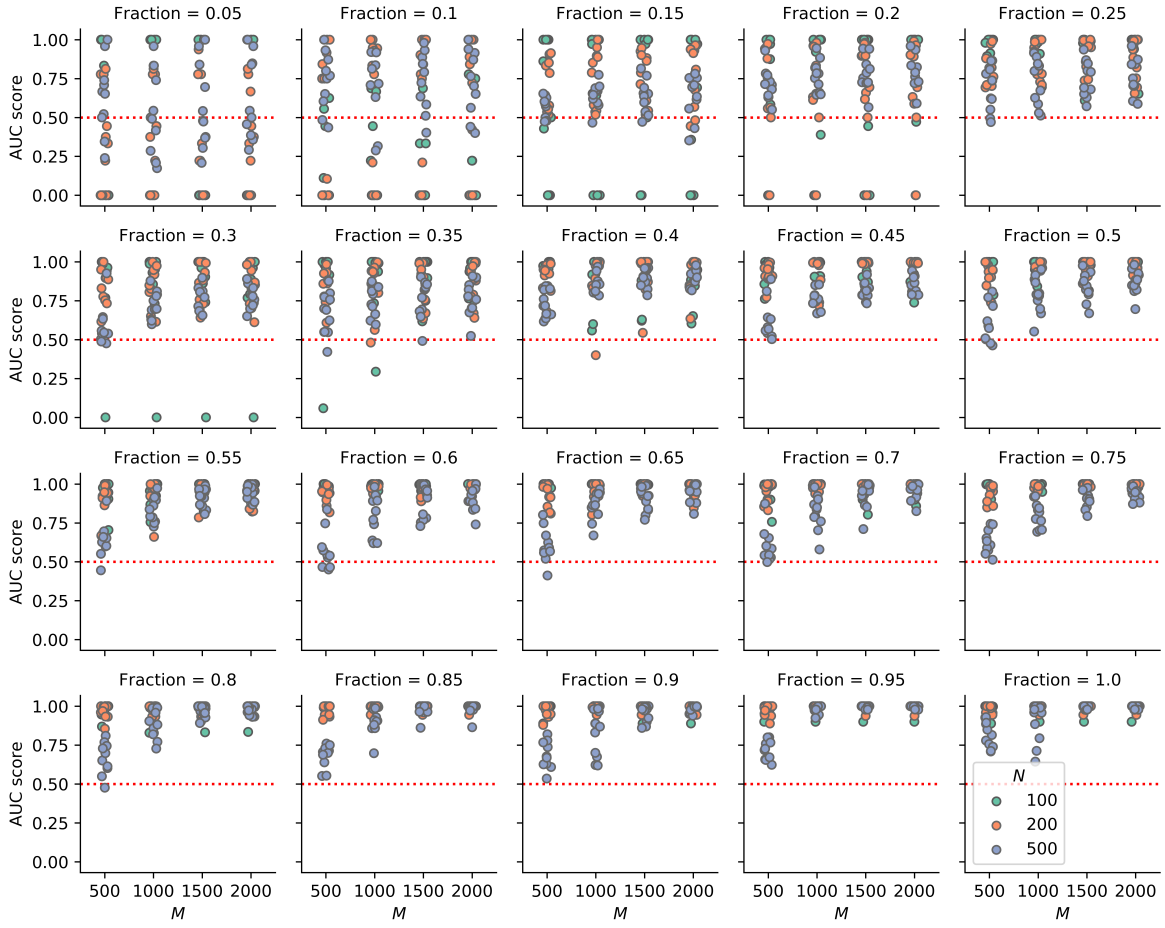

Figure S2. **Feasibility of reconstruction in networks with only a fraction of observable units.** Larger fractions of observed units and larger number recorded events improve quality of reconstruction. Quality of reconstruction versus number of recorded events M for networks of LIF-δ neurons of $N \in \{100, 200, 500\}$ with half excitatory and half inhibitory connections, $J_{\text{exc}} = 0.5$ mV, $J_{\text{inh}} = -J_{\text{exc}}$, and transmission delays $\tau = 1.5$ ms. The input currents were randomly selected from the uniform distribution $I_i \in [1.2, 1.4]$ pA for all $i \in \{1, 2, \ldots, N\}$ and the connection probability was set to $p = 0.1$.

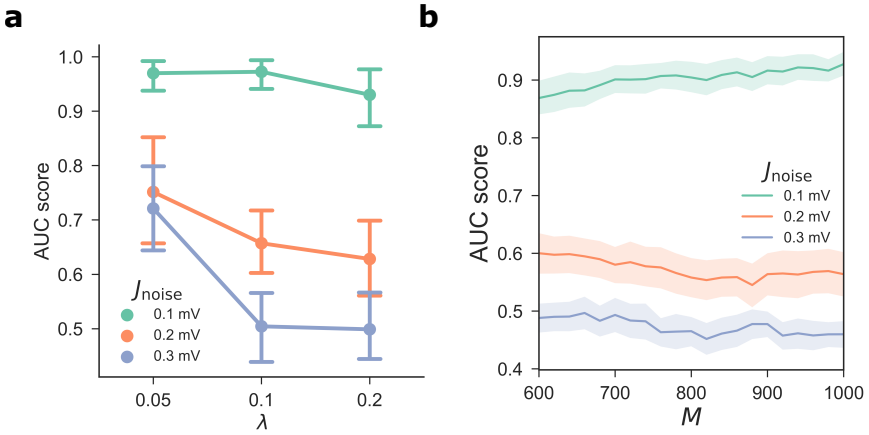

Figure S3. **Increasing sizes of recording data compensates for distractions by external noise.** Reconstructions of networks of $N = 100$ LIF neurons having δ-synapses with $N_{exc} = 80$ and, $N_{inh} = 20$. The weight for excitatory synapses was set to $J_{exc} = 0.3\,\mathrm{mV}$ and for inhibitory synapses to $J_{inh} = -4J_{exc}$. The connection probability was set to $p = 0.1$ and the simulation time to 50 s. The input currents were selected from $I_i \in \mathcal{U}(1.2, 1.4)$ pA. **a**, Quality of reconstruction versus relative frequency λ for $J_{noise} \in \{0.1, 0.2, 0.3\}$ mV. **b**, Quality of reconstruction versus number of events M for $J_{noise} \in \{0.1, 0.2, 0.3\}$ mV and $\lambda = 0.2$.

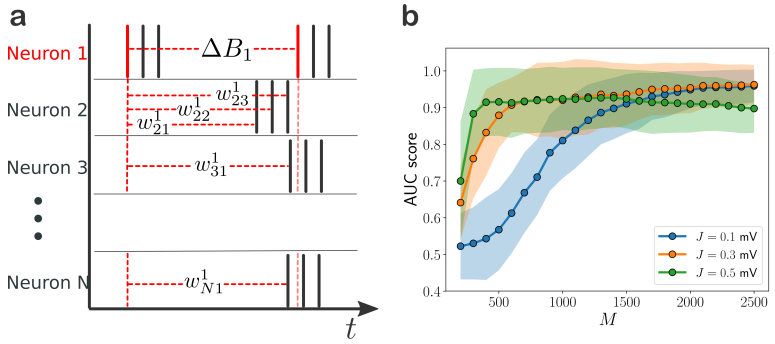

Figure S4. **Bursting period replaces inter-spike intervals for connectivity inference in bursting settings.** (**a**) Schematics of an event for a sample unit ($i = 1$)formed by the interval between two successive burst onsets of unit 1 and all cross-event intervals that may influence the subsequent burst onset of unit 1. (b) Quality of reconstruction versus the number of events M considered for networks of $N = 50$ aEIF neurons exhibiting bursting activity for three different interaction strengths J .

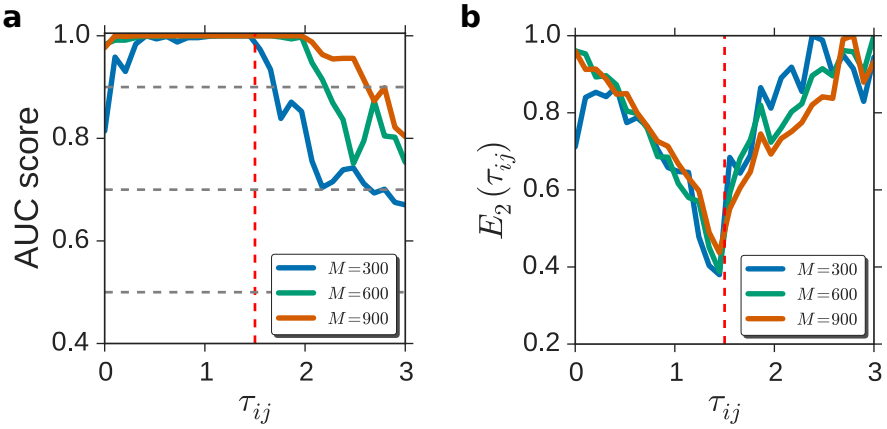

Figure S5. **Reconstructions are robust against misestimation of transmission delays.** Reconstructions of networks of $N = 100$ LIF neurons having δ-synapses with $N_{\text{exc}} = 75$ and, $N_{\text{inh}} = 25$. The weight for excitatory synapses was set to $J_{\text{exc}} = 0.5\,\text{mV}$ and for inhibitory synapses to $J_{\text{inh}} = -5J_{\text{exc}}$. The connection probability was set to $p = 0.1$ and the simulation time to 50 s. The input currents were selected from $I_i \in \mathcal{U}(1.2, 1.4)$ pA. (**a**,**b**), Quality of reconstruction and error function (10) versus employed transmission delay τ_{ij}. The vertical dashed line indicates the actual delay $\tau^*_{ij} = 1.5\,\text{ms}$.